RSC Advances

ROYAL SOCIETY OF CHEMISTRY

www.rsc.org/advances

Journal Name

ARTICLE

High-performance capacitive behavior of layered reduced graphene oxide and polyindole nanocomposite materials

Qianjie Zhou [a], Danhua Zhu [a], Xiumei Ma [a], Jingkun Xu [a, *], Weiqiang Zhou [b, *], Feng Zhao [a]

In this work, a high-capacitance hybrid nanocomposite based on reduced graphene oxide (RGO) and polyindole (PIn) was fabricated via an *in-situ* chemical oxidative polymerization approach. The structure and morphology of PIn/RGO were investigated by FT-IR, Raman spectrum, SEM and TEM, respectively. The electrochemical properties of this electrode in aqueous H_2SO_4 electrolyte were also investigated by cyclic voltammetry, galvanostatic charge/discharge, and electrochemical impedance spectroscopy (EIS). Compared to RGO and PIn electrodes, the PIn/RGO hybrid nanocomposite shows a large improved specific capacitance of 322.8 F g^{-1} at 1.0 A g^{-1}, good stability with a cycling efficiency of 94.5% after 1000 cycles, and high energy density of 36 Wh kg^{-1} at high power density of 5000 W kg^{-1}. The enhanced performance is proposed to arise from the synergetic effect between PIn and RGO. In addition, the symmetric PIn/RGO//PIn/RGO supercapacitor showed specific capacitance of 99.8 F g^{-1} and only 3.7% decay after 1000 cycles. These results implied that PIn/RGO should be a promising electrode material for supercapacitor applications.

Introduction

Nowadays, with the increasing demand for energy and growing concerns about air pollution caused by over-exploitation of fossil fuel, the development of energy storage devices is gaining more and more interest.[1-3] Supercapacitors, one of the most promising candidates for flexible energy storage devices, have attracted significant research due to their high power density, fast charging-discharging process, long cycle life, and environmental friendliness.[4-7] According to the energy storage mechanism, supercapacitors can be divided into the electrical double-layer capacitors (EDLCs) based on carbonaceous materials[8-11] and the pseudo-capacitors (PCs) based on metal oxides

or conducting polymers (CPs).[12,19] EDLCs show high power density and long cycle life, but their specific capacitance and energy density are unsatisfactory.[20] However, PCs possess high specific capacitance and high energy density with low cycle stability.[21] Currently, one of the most important aspects in the development of supercapacitors is to construct novel materials that combine high energy density, high power capability and long cycle life.

To satisfy such a multiple requirement, lots of advanced materials based on graphene, such as heteroatom-doped graphene, graphene/metal oxides or graphene/CPs binary composites, and graphene/CPs/metal oxides ternary composites, have been widely

prepared, in which the mechanism of electrostatic charge accumulation is coupled with that of redox reaction.[22,23] Among the wide variety of multifunctional materials, the preparation of graphene/CPs binary composites is more simple and cost-effective. For example, Zhang *et al.* prepared the graphene/polyaniline composites by *in-situ* polymerization of aniline monomer in the presence of graphene oxide. The specific capacitance of the optimized graphene/polyaniline composites was 210 F g^{-1} at 1.0 A g^{-1}.[24] Zhang and Zhao prepared polypyrrole/RGO (PPy/RGO) nanocomposites via an *in-situ* polymerization method, the specific capacitances was 204 F g^{-1} at 1.0 A g^{-1}.[25] However, cycling instability is still a major obstacle for practical applications due to the structural instability of polyaniline and PPy resulting from the degradation and repeated volumetric swelling/shrinking during charge/discharge process. For example, Wang *et al.* reported that PANI deposited on coral-like monolithic carbon can achieve high capacitance retention of 78.2% after 1000 cycles at a scan rate of 100 mV s^{-1}.[26] Qian *et al.* demonstrated that PPy/RGO core-shell composite can retain 85% of capacitance after testing for 1000 cycles at 0.5 A g^{-1}.[27] Among CPs, polyindole (PIn) belonging to the fused-ring family has been rapidly increasing. Due to close structural similarities to poly(para-phenylene) and polypyrrole, PIn possesses properties of both compounds. Additionally, PIn has superior thermal stabilities compared to polyaniline, polypyrrole, and polythiophene.[28,29] Especially, PIn is an electrochemically stable redox material, which may run over more than 450000 redox cycles at between -0.5 and 0.9 V *vs.* SCE.[30]

Therefore, the high stability of PIn should be considered as a significant advantage in supercapacitors. At present, PIn applied in supercapacitors has also received attention,[31,32] but the reports available in the literature are scarce mainly due to the low conductivity of PIn.

Due to the presence of N-H group on indole units, PIn can combine with RGO through the interaction of functional groups, forming high-stability composites. The introduction of RGO into PIn can greatly enhance the conductivity of PIn. Herein, we attempted and successfully prepared hybrid nanocomposite based on RGO and PIn by using an *in-situ* chemical oxidative polymerization approach. The structures, morphologies and capacitance properties of as-synthesized PIn/RGO were characterized in detail. It is found that PIn/RGO hybrid nanocomposite showed an enhanced capacitance performance without deteriorating the cycle life compared to RGO and PIn.

Experimental details

Materials

Graphene oxide was obtained from Nanjing XFNANO Materials Tech Co., Ltd. Indole (99% purity) and ammonium peroxodisulfate (APS) were obtained from Shanghai Vita Chemical Reagent Co., Ltd. China. Hydrazine hydrate (HHA) and ammonium hydroxide were purchased from Tianjing Bodi Chemical Reagent Co., Ltd. and Aladdin Industrial Corporation, respectively. Absolute ethyl alcohol was bought from Xilong Chemical Industry Incorporated Co. Ltd.

Conductive carbon cloth (CC, WOS1002, Ce Tech) was purchased from Phychemi Company Limited, China. Sulfuric acid (98%) was purchased from Jinan Chemical Regant Co., Ltd. Double deionized water was used in the experiment.

Preparation of PIn, RGO and PIn/RGO electrodes

RGO sheets were prepared by followed method: A 2.3 g L^{-1} GO ethanol suspension was obtained by ultrasonication for 2 h. After that 1 mL $NH_3 \cdot H_2O$ was added to the suspension, followed by magnetic stirring for 10 min and then kept at 100 ^{o}C for 12 h. After the solution was fully cooled, washed with ethanol and double deionized water, then dried at 60 ^{o}C in a vacuum oven for 3 days, RGO powder were obtained.

PIn/RGO were synthesized by using a typical *in-situ* chemical oxidative polymerization approach. Namely, 0.1 M indole monomer was added into the RGO suspension and stirred for 10 min to form a uniform mixture. The 0.2 M APS was resolved in H_2O solution, then added into the suspension containing monomer and RGO. The mixture was sustained overnight under stirring. The resulting precipitates were washed with ethanol and double deionized water, then dried at 60 ^{o}C in a vacuum oven for 3 days. The synthesis of PIn was carried out by the above procedures without adding RGO.

A small amount of ethanol was added into PIn, RGO or PIn/RGO to form a slurry, then the slurry was coated on a carbon cloth sheet (10 mm × 10 mm × 1.0 mm), which is defined as PIn/CC, RGO/CC and PIn/RGO/CC electrodes, respectively. All electrodes were dried at 60 ^{o}C in a vacuum oven for 24 h. The mass loading of active material on each electrode was controlled to be ca. 0.1 mg.

Characterizations

FT-IR spectra were recorded using a Bruker Vertex 70 Fourier transform infrared spectrometer. Raman spectra were taken in a back scattering configuration using a Jobin Ycon Horiba Lab Ram HR800 Raman system. Scanning electron microscopy (SEM) images were carried out by Hitachi-S4800 microscope. Transmission electron microscopy (TEM) images were obtained on FEI TECNAI G2 F20 microscope at an acceleration voltage of 200 kV. X-ray diffraction (XRD) analysis was performed by a D8 Advance instrument.

All the electrochemical characterizations were carried out in 1.0 M H_2SO_4 using a one-compartment cell with electrochemical workstation (model CHI660E, Shanghai Chenhua Instrumental Co., Ltd., China). Active material modified CC was used as working electrode, and a platinum wire (1 mm diameter) and a saturated calomel electrode (SCE) were used as the auxiliary electrode and the reference electrode, respectively. The mass loading of active material on CC substrate was weighed by an electronic microbalance (Mettler-Toledo/XS205, up to 0.01 mg).

Results and discussion

Structure and morphology

Journal Name

ARTICLE
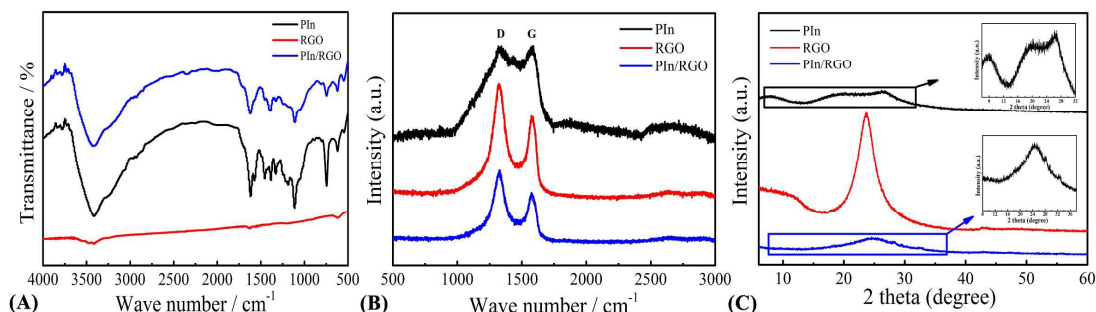
Fig. 1 FT-IR (A), Raman (B) and XRD (C) spectrum of PIn, RGO and PIn/RGO.

The structure of the PIn, RGO and PIn/RGO samples were investigated using FT-IR, Raman and XRD. As shown in Fig. 1A, the featureless FT-IR spectrum of RGO indicated that the chemical reduction of GO was relatively completed with few oxygen-containing groups such as -C=O and -C-O groups, which is difficult to be completely reduced.[33] The spectrum of PIn/RGO displayed the same but weak peaks as PIn at 744, 1111, 1456, 1616, and 3420 cm^{-1}, which correspond to -C-H, -C-N, -C-C, -C=C, and -N-H stretching vibrations, respectively.[34-36] In Fig. 1B, the two Raman bands of PIn at about 1326 and 1582 cm^{-1} can be ascribed to stretching vibrations of pyrrole ring and phenyl ring.[37-39] The typical D-band and G-band of RGO were also distinctly observed at 1323 and 1582 cm^{-1}, respectively. The D-band is associated with the vibrations of sp^2 carbon atoms due to the breathing mode of aromatic rings, whereas the G-band corresponded to the E_{2g} mode for the bond stretching of sp^2 carbon pairs in both rings and chains.[40] The second

order zone boundary phonon, 2D band, does not satisfy the Raman fundamental selection rule and is not seen in defect-rich graphene.[41] Therefore, the 2D band is absent in the Raman spectra of our samples prepared by chemically reduced method. And the spectrum of PIn/RGO is similar to that of RGO, suggesting that the introduction of PIn particles will not affect the structure of RGO sheets. However, the intensity ratio of D-band to G-band increased from 1.27 of RGO to 1.50 of PIn/RGO, which was attributed to the effective interaction between PIn and RGO. In Fig. 1C, the XRD spectra of PIn shows two bands at $2\theta = 20°$ and $26°$, and one unusual sharp peak around $2\theta = 8°$ which is can be assigned to the periodic distance between the dopant and the nitrogen atom of the adjacent main chain that fits well with reported results.[42] An XRD pattern of the GO films exhibits a single peak at around $11°$ and the most intense peak (002) for graphite at $2\theta = 26.50°$.[43] The RGO sample does not have the same peak ($\approx 11°$) in XRD pattern but remains a broad peak at 2θ between

20° and 30°, which indicates the existence of weak π-π stacking between the RGO sheets due to the crumpled and poorly ordered structure.[44] In the case of the PIn/RGO composite, a new broad peak at $2\theta = 25°$ can be found, indicating the formation of PIn on the surface of RGO. The RGO is further confirmed by X-ray photoelectric spectroscopy (XPS) (in Fig. S1). The C1s signals contributed by the C=O and C-O groups were significantly reduction and RGO exhibited a peak at 285.8 eV, which indicates that the successful reduction of graphene oxide.[33]
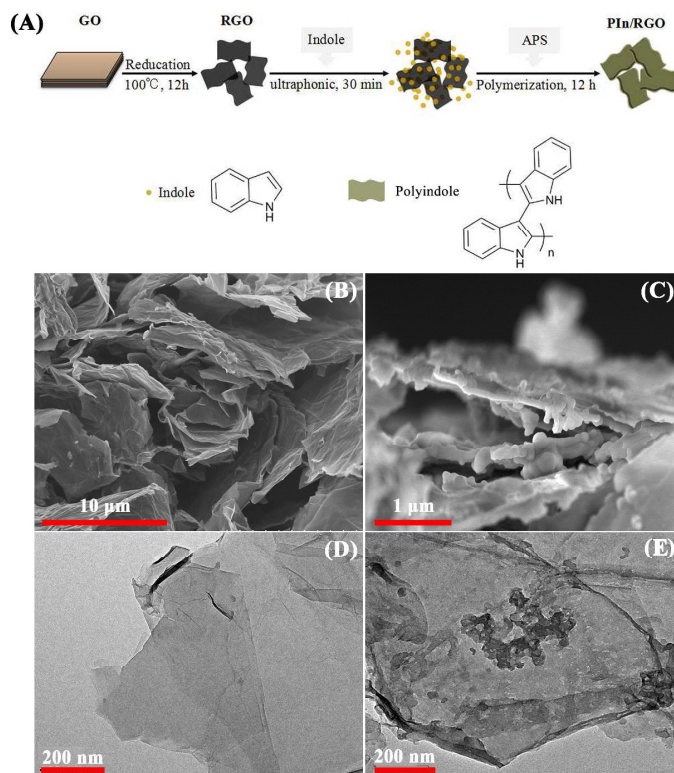
Fig. 2 (A) Schematic illustration of the formation process of the PIn/RGO composite; SEM and TEM images of RGO (B&D) and PIn/RGO (C&E).

The schematic illustration of the preparation of the PIn/RGO is illustrated in Fig. 2A, where the PIn nanoparticle are directly grown on the surface of RGO. After the chemical reduction of GO, as-formed RGO sheets showed distinct crumpled structures and maintain the 2D geometry (Fig. 2B), which is different from the GO seen from SEM in Fig. S2. In addition, PIn was hollow nanosphere evidenced by the sharp contrast between the dark edge and the pale center in the TEM images (Fig. S3). However, the shape of PIn formed on RGO became nanoparticles (Fig. 2C). This is due to the indole monomers beforehand adsorbed at surface of RGO polymerized into small nanoparticle as seeds. With increasing of reaction time, the seeds grew up gradually, finally formed PIn nanoparticle structure. In comparison with the TEM images of RGO and PIn/RGO (Fig. 2D&E), it can be distinctly observed that PIn nanoparticles have been distributed at the two sides of RGO, forming sandwich PIn/RGO hybrid nanocomposite.

Electrochemical evaluation

Journal Name

ARTICLE
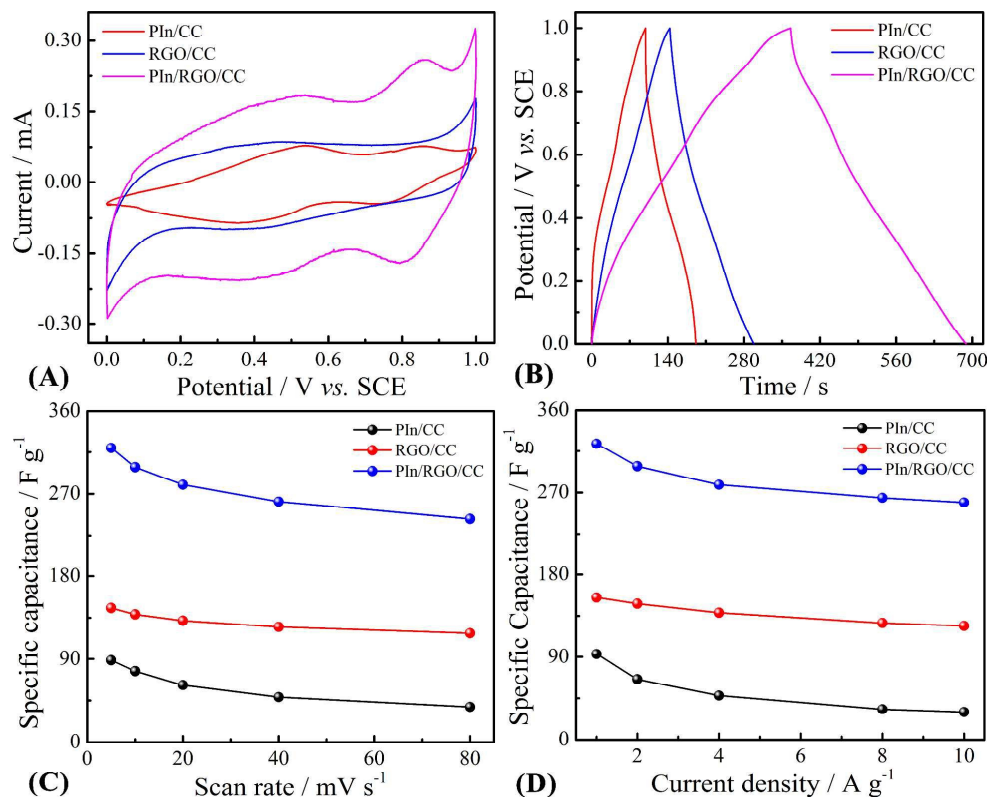
Fig. 3 Electrochemical test of the PIn/CC, RGO/CC and PIn/RGO/CC electrodes in 1.0 M H_2SO_4 solution: (A) cyclic voltammograms at 5 mV s^{-1}, (B) galvanostatic charge-discharge curves at 1.0 A g^{-1}, (C) specific capacitance as a function of scan rates, and (D) specific capacitance as a function of current densities.
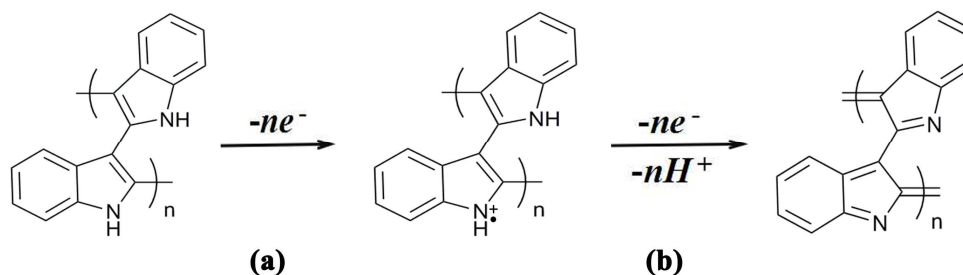
Scheme 1. Structural conversions of PIn electrode in sulfuric acid solution: (a) electronic exchange in the first redox process; (b) concomitant proton and electron exchange in the second redox.

It is well-known that CC possesses high strength, low density and high electrical conductivity. It consists of many carbon fibers that

arranged crosswise to form a 3-D structure with numerous spaces (Fig. S4). The 3-D structure not only facilitates the diffusion of electrolyte into the active materials but also accelerates the ion transport. Therefore, CC was selected as the substrate of PIn/RGO active materials for the fabrication of high-performance electrode. To evaluate the electrochemical properties of the PIn/CC, RGO/CC and PIn/RGO/CC electrodes, the measurements of the cyclic voltammograms (CV) at different scan rates vary between 5 and 80 mV s^{-1} and the galvanostatic charge-discharge (GCD) at different current densities from 1 to 10 A g^{-1} were conducted in 1.0 M H$_2$SO$_4$ aqueous electrolyte (Fig. S5). The shapes of the CV curves of PIn/CC, RGO/CC and PIn/RGO/CC electrodes did not obviously change, implying the good rate capability of the electrodes. In Fig. 3A, the RGO/CC shows a typical rectangular curve similar to the CV of conventional carbon materials. The pure PIn/CC electrode exhibits two couple of anodic and cathodic peaks, which distinguished from that of electric double layer capacitance, indicating the charge capability of PIn electrode is through the process of electro-oxidation and electro-reduction. In **Scheme 1**, we provided the structural conversions of PIn in sulfuric acid solution. During the first redox process, electronic exchange and the radical cationic species coexist, it can be concluded that the neutral species are converted to radical-cation as the oxidation proceeds. On the contrary, concomitant proton and electron exchange related to the redox transformation occurring at the most positive potentials during the second redox process.[45] The CV of PIn/RGO/CC combines the

features of RGO and PIn. The oxidation and reduction peaks of PIn/RGO were at 0.52 V, 0.86 V and 0.4 V, 0.8 V, respectively. The slightly shift of peaks was mainly due to the interaction of functional groups on PIn and RGO, which affected the intrinsically electrochemical property of PIn. However, the capacitive performance of CC was very small and even negligible compared with those of the PIn and PIn/RGO (Fig. S6). In Fig. 3B, the GCD curves of these electrodes were similar in shape between 0 and 1.0 V. Typical triangular curves show distinct capacitance characteristics of the three electrodes. Furthermore, the PIn/RGO/CC electrode has a longer charge and discharge time than those of the PIn/CC and RGO/CC electrodes, which indicates that PIn/RGO/CC had a higher specific capacitance.

In order to further reveal the change trend of specific capacitance with the increase of scan rate and current density, the functions between specific capacitance and scan rate and current density were plotted as Fig. 3C&D, respectively. The specific capacitance values (C) of the active materials were calculated from the cyclic voltammograms and the charge-discharge methods by means of *Eq.* (1) and (2):[34]

$$C = \frac{\int_{E_1}^{E_2} i(E)d(E)}{2vm(E_2 - E_1)} \qquad (1)$$

$$C = \frac{It}{mv} \qquad (2)$$

where *C* is specific capacitance (F g^{-1}), E_1 and E_2 are the cutoff potentials in cyclic voltammetry, $i(E)$ is the instantaneous current,

$\int_{E1}^{E2} i(E)d(E)$ is the total voltammetric charge obtained by integration of the positive and negative sweeps in the cyclic voltammograms, I and t are the discharge current and time, respectively, v is the scan rate, and m is the mass of the individual sample. As shown in Fig. 3C, at a scan rate of 5 mV s^{-1}, the specific capacitance of the PIn/CC was only 88.7 F g^{-1}. This is due to the extremely low conductivity of PIn (1.5×10^{-5} S cm^{-1}) hinders the charges transfer in adjacent PIn particles and inside PIn particles, which greatly limits the pseudocapacitance of PIn. When the PIn was combined with RGO with high conductivity (6.1 S cm^{-1}), the as-formed PIn/RGO composite showed enhanced conductivity of 0.2 S cm^{-1} relative to that of PIn, and the specific capacitance of the PIn/RGO electrode reached 319.4 F g^{-1}, which was higher than that of the RGO/CC (145.3 F g^{-1}) electrode. Therefore, the high conductivity favors the redox reaction of PIn component, which can enhance the pseudocapacitance of PIn in the composite. It can be also seen from Fig. 3D, the specific capacitance of PIn/RGO/CC (322.8 F g^{-1}) electrode at 1.0 A g^{-1} was superior to those of PIn/CC (93.0 F g^{-1}) and RGO/CC (154.7 F g^{-1}) electrodes. On the other hand, the specific capacitance of PIn/RGO/CC is about 2.6 times as high as the average value [(154.7 + 93)/2 = 123.85 F g^{-1}] of PIn/CC and RGO/CC, indicating the synergic effect of both components. The synergic effect mainly came from below aspects: (1) the enhanced conductivity of PIn promoted the electrochemical activity; (2) the interaction of functional groups on PIn and RGO affected the surface/interface microscopic structures and properties of composites,

which was beneficial to improve the specific capacitance. Here, note that the synergic effect did not arise from the aspect of the specific surface area due to the specific surface area of PIn/RGO composite (28.45 m^2 g^{-1}) was smaller than those of individual PIn (68.39 m^2 g^{-1}) and RGO (48.37 m^2 g^{-1}).
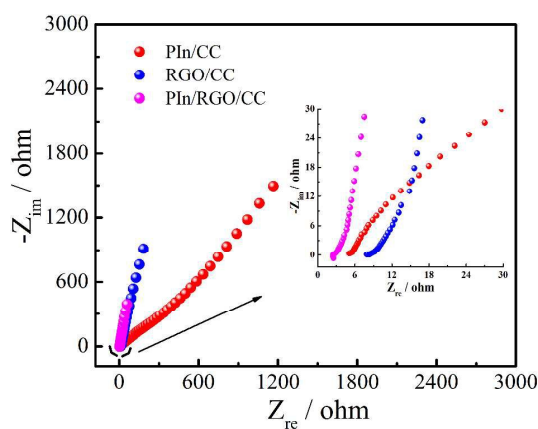
Fig. 4 Nyquist plots of PIn/CC, RGO/CC and PIn/RGO/CC electrodes in 1.0 M H$_2$SO$_4$ solution.

The capacitance performance of the PIn/CC, RGO/CC and PIn/RGO/CC electrodes were also investigated by the electrochemical impedance spectroscopy (EIS). Fig. 4 shows the Nyquist curves of PIn/CC, RGO/CC and PIn/RGO/CC electrodes. The PIn/RGO/CC shows a near-vertical curve in the low frequency region, indicating good capacitor behavior. In the high frequency region (inset in Fig. 4), PIn/RGO/CC showed a smaller semicircle and x-intercept compared to PIn/CC and RGO/CC, suggesting a facilitated electronic/ionic transfer for PIn/RGO/CC. The low x-intercept of PIn/RGO/CC is mainly due to the lower resistance between the ion and material, and the good intrinsic electronic properties of the material. Additionally, it was observed from the data

at 0.01 Hz, the PIn/CC had a large $|-Z_{im}|$ value, whereas the $|-Z_{im}|$ value of PIn/RGO/CC was markedly decreased. This implied that the

specific capacitance of PIn/RGO/CC electrode was significantly improved.
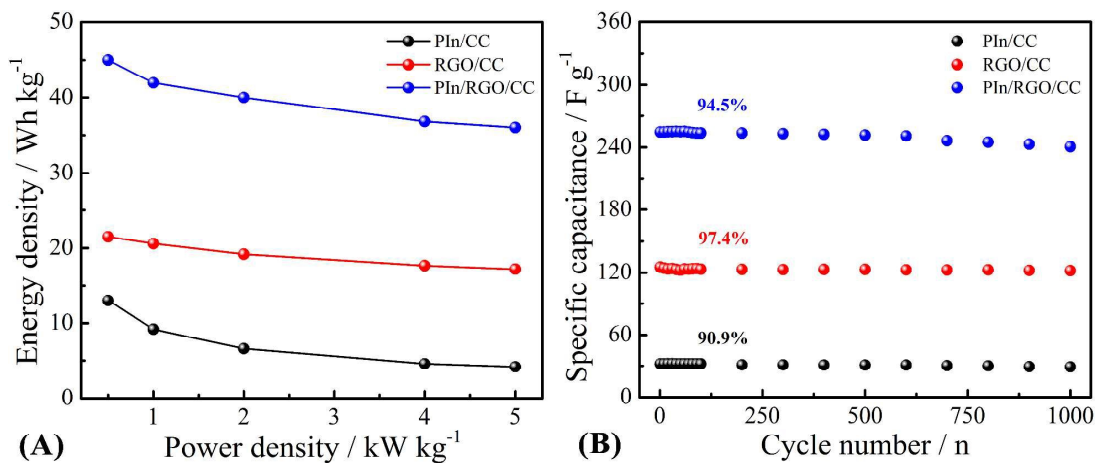
Fig. 5 Electrochemical test of the PIn/CC, RGO/CC and PIn/RGO/CC electrodes in 1.0 M H_2SO_4 solution: (A) power densities as a function of energy densities; (B) galvanostatic charge-discharge life during 1000 cycles at a current density of 10 A g^{-1}.

The Ragone plot showing the energy density and power density is presented in Fig. 5A. The power density (P, W kg^{-1}) and energy density (E, Wh kg^{-1}) values were calculated by the following *Eq*. (3) and (4).[34]

$$E = \frac{1}{2}CV^2 \qquad (3)$$

$$P = \frac{E}{\Delta t} \qquad (4)$$

Where C is the specific capacitance of the electrode (F g^{-1}), V is the voltage window (V), and Δt is the discharge time (s). Their energy density decreases slowly as the power density increases. When the power density was 500 W kg^{-1}, the energy density remains was 45 Wh kg^{-1} for the PIn/RGO/CC electrode, which was higher than those of PIn/CC (13 Wh kg^{-1}) and RGO/CC (21.5 Wh kg^{-1}) electrodes.

Even at a high power density of 5000 W kg^{-1}, PIn/RGO/CC electrode still shows a high energy density of 36 Wh kg^{-1}. Such results indicated that the PIn/RGO/CC had high energy density and high power density and will have promising applications in the field of electrochemical energy storage.

Cyclic stability is another important aspect of the potential application of supercapacitors. The cyclic stabilities of the electrodes were examined by consecutive galvanostatic charge/discharge measurements at a current density of 10 A g^{-1}, the results were shown in Fig. 5B. The RGO/CC electrode shows excellent cyclic stability (97.4% capacitance retention) after 1000 cycles due to the stable nature of the carbonaceous materials. The PIn/CC shows 90.9% of the original capacitance is retained after 1000 cycles. PIn/RGO/CC

shows an enhanced cyclic stability compared with that of PIn/CC, and the capacitance can retain 94.5% of its original value after 1000 charge/discharge cycles. These results indicated that the cyclic stability of PIn/RGO hybrid nanocomposite was still comparable with RGO materials. The cycle stabilities of PIn and PIn/RGO hybrid nanocomposite were also compared with several important RGO/CPs composites as shown in Table 1. As seen from Table 1, PIn/RGO hybrid nanocomposite has higher cycle stability and comparable specific capacitance.

Table 1 Specific capacitance and cycle stability comparison of PIn/RGO with several important RGO/CPs composites.

CPs/RGO	Scan rate or current density	Specific capacitance / F g^{-1}	Capacitance retention after cycle test	Ref.
RGO/PEDOT	0.5 A g^{-1}	104	88% after 1000 cycles	25
RGO/PPy	0.5 A g^{-1}	229	81% after 1000 cycles	25
RGO/PANI	0.5 A g^{-1}	349	82% after 1000 cycles	25
RGO/PANI	0.5 A g^{-1}	284	70% after 1000 cycles	24
RGO/PANI	2 mV s^{-1}	207.11	75% after 1000 cycles	46
RGO/PEDOT	0.5 A g^{-1}	270	93% after 10000 cycles	47
RGO/RuO$_2$/PEDOT	1 mV s^{-1}	184	70% after 5000 cycles	48
SG/PPy	0.5 A g^{-1}	285	92% after 1000 cycles	49
G/PTh	1 mV s^{-1}	176	88% after 100 cycles	50
PIn	1 A g^{-1}	93.0	90.9% after 100 cycles	This work
RGO/PIn	1 A g^{-1}	322.8	94.5% after 1000 cycles	This work

Journal Name

ARTICLE
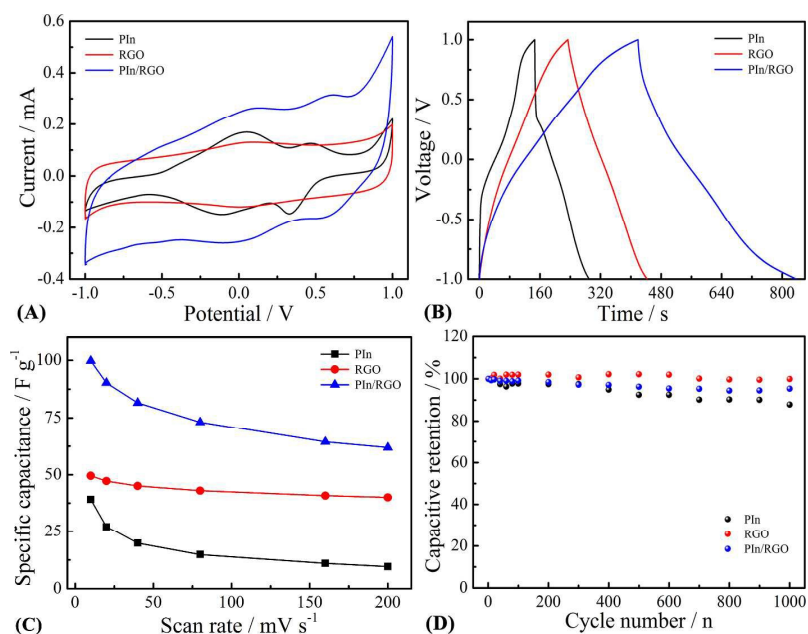
Fig. 6 Electrochemical performance of symmetric supercapacitor based on two identical electrodes (PIn//PIn, RGO//RGO and PIn/RGO//PIn/RGO) in 1.0 M H_2SO_4 solution. (A) CV curves at a scan rate of 10 mV s^{-1}, (B) GCD curves at a current density of 0.5 A g^{-1}, (C) specific capacitance as a function of scan rates, and (D) galvanostatic charge-discharge life during 1000 cycles at a current density of 10 A g^{-1}.

The performances of the symmetric supercapacitors based on two identical electrodes were evaluated by means of CV, GCD and cycling-life test. The CV at different scan rates varied between 10 and 200 mV s^{-1} and the GCD at different current densities was conducted from 0.5 to 10 A g^{-1} (Fig. S7). In Fig. 6A, the CVs of PIn//PIn and PIn/RGO//PIn/RGO exhibit two pairs of redox waves which are attributed to the redox of PIn. By comparison, the CV of RGO//RGO exhibits a rectangular area. In Fig. 6B, the "IR drop" decreases in the order of PIn//PIn, PIn/RGO//PIn/RGO and

RGO//RGO. This indicated that RGO could improve the conductivity of PIn and reduce the internal resistance of electrodes. Fig. 6C shows the specific capacitance as a function of scan rates. When the scan rates increased from 10 mV s^{-1} to 200 mV s^{-1}, the capacitance retention of PIn/RGO//PIn/RGO is 62.1%, which is much higher than that of PIn//PIn (26.7%) but lower than that of RGO//RGO (81.6%). As shown in Fig. 6D, the specific capacitance loss of PIn//PIn reaches 12.3% after 1000 cycles at a current 10 A g^{-1}. However, the PIn/RGO//PIn/RGO shows 3.7% decay. Above results illustrate that

RGO can improve the capacitance performance of PIn including specific capacitance, rate capability and cycle life.

Conclusions

In summary, a novel PIn/RGO hybrid nanocomposite has been prepared by simple *in-situ* chemical oxidative polymerization in ethanol solvent. The electrochemical properties revealed an excellent capacitive performance of PIn/RGO/CC. The specific capacitance of PIn/RGO/CC electrode was measured to be as high as 322.8 F g^{-1} at a current density of 1.0 A g^{-1}. And the energy density of PIn/RGO/CC reached 36 Wh kg^{-1} at high power density of 5000 W kg^{-1}. At the same time, the capacitive retention of PIn/RGO/CC was 94.5% after 1000 cycles, which was comparable with RGO/CC. In addition, the symmetric PIn/RGO//PIn/RGO supercapacitor showed higher specific capacitance without deteriorating the cycle life compared to PIn//PIn and RGO//RGO. The good capacitive performance of the PIn/RGO composite is attributed to the contribution of both double layer capacitance and pseudocapacitance, together with the synergic effect of RGO and PIn in the composite.

Acknowledgement

Notes and references

[a] Jiangxi Key Laboratory of Organic Chemistry, Jiangxi Science and Technology Normal University, Nanchang, 330013, P. R. China

[b] Chemistry and Chemical Engineering College, Jiangxi Science and Technology Normal University, Nanchang 330013, PR China

* Corresponding author: Fax: +86-791-83823320, Tel.: +86-791-88537967, E-mail: xujingkun@tsinghua.org.cn; zhouwqh@163.com

1   R. Li, B. Nie, P. Digiglio and T. Pan, *Adv. Funct. Mater.*, 2014, **24**, 6195-6203.

2   F. Béguin, V. Presser, A. Balducci and E. Frackowiak, *Adv. Mater.*, 2014, **26**, 2219-2251.

3   K. Naoi, W. Naoi, S. Aoyagi, J. I. Miyamoto and T. Kamino, *Acc. Chem. Res.*, 2012, **46**, 1075-1083.

4   L. L. Zhang and X. S. Zhao, *Chem. Soc. Rev.*, 2009, **38**, 2520-2531.

5   E. Frackowiak, *Phys. Chem. Chem. Phys.*, 2007, **9**, 1774-1785.

6   P. Simon and Y. Gogotsi, *Nat. Mater.*, 2008, **7**, 845-854.

7   Y. Xiao, C. Long, M. T. Zheng, H. W. Dong, B. F. Lei, H. R. Zhang and Y. L. Liu, *Chinese Chem. Lett.*, 2014, **25**, 865-868.

8   J. L. Liu, L. L. Zhang, H. B. Wu, J. Y. Lin, Z. X. Shen and X. W. Lou, *Energ. Environ. Sci.*, 2014, **7**, 3709-3719.

9   S. Bose, T. A. Kuila, K. Mishra, R. Rajasekar, N. H. Kim and J.

H. Lee, *J. Mater. Chem.*, 2012, **22**, 767-784.

10　L. M. Dai, D. W. Chang, J. B. Baek and W. Lu, *Small*, 2012, **8**, 1130-1166.

11　C. W. Huang, Y. T. Wu, C. C. Hu and Y. Y. Li, *J. Power Sources*, 2007, **172**, 460-467.

12　Z. B. Lei, J. T. Zhang and X. S. Zhao, *J. Mater. Chem.*, 2012, **22**, 153-160.

13　C. C. Hu and W. C. Chen, *Electrochim. Acta*, 2004, **49**, 3469-3477.

14　T. Y. Dai, R. Tang, X. X. Yue and L. Xu, *Chinese J. Polym. Sci.*, 2015, 33, 1018-1027.

15　F. Fusalba, P. Gouérec, D. Villers and D. Belanger, *J. Electrochem. Soc.*, 2001, 148, A1-A6.

16　C. C. Hu and X. X. Lin, *J. Electrochem. Soc.*, 2002, 149, A1049-A1057.

17　J. P. Ferraris, M. M. Eissa, I. D. Brotherston, D. C. Loveday and A. A. Moxey, *J. Electroanal. Chem.*, 1998, **459**, 57-69.

18　R. I. Jaidev, A. K. Jafri, S. Mishra and Ramaprabhu, *J. Mater. Chem.*, 2011, **21**, 17601-17605.

19　X. M. Ma, W. Q. Zhou, D. Z. Mo, K. X. Zhang, Z. P. Wang, F. X. Jiang, D. F. Hu, L. Q. Dong and J. K. Xu, *J. Electroanal. Chem.*, 2015, **743**, 53-59.

20　J. Wei, G. Xing, L. Gao, H. Suo, X. He, C. Zhao and S. Xing, *New J. Chem.*, 2013, **37**, 337-341.

21　I. Kovalenko, D. G. Bucknall and G. Yushin, *Adv. Funct. Mater.*, 2010, **20**, 3979-3986.

22　S. Stankovich, D. A. Dikin, G. H. Dommett, K. M. Kohlhaas, E. J. Zimney, E. A. Stach and R. S. Ruoff, *Nature*, 2006, **442**, 282-286.

23　Y. Shao, M. F. El-Kady, L. J. Wang, Q. Zhang, Y. Li, H. Wang and R. B. Kaner, *Chem. Soc. Rev.*, 2015, **44**, 3639-3665.

24　K. Zhang, L. L. Zhang, X. S. Zhao and J. Wu, *Chem. Mater.*, 2010, **22**, 1392-1401.

25　J. Zhang and X. S. Zhao, *J. Phys. Chem. C*, 2012, **116**, 5420-5426

26　Y. Wang, S. Tao, Y. An, S. Wu and C. Meng, *J. Mater. Chem. A*, 2013, **1**, 8876-8887.

27　T. Qian, C. Yu, S. Wu and J. Shen, *J. Mater. Chem. A*, 2013, **1**, 6539-6542.

28　P. S. Abthagir, K. Dhanalakshmi and R. Saraswathi, *Synth. Met.*, 1998, **93**, 1-7.

29　S. Palaniappan and B. H. Narayana, *Thermochim. Acta*, 1994, **237**, 91-97.

30　E. B. Maarouf, D. Billaud and E. Hannecart, *Mater. Res. Bull.*, 1994, **29**, 637-643.

31　R. Pavul Raj, P. Ragupathy and S. Mohan. *J. Mater. Chem. A*, 2015, **3**, 24338-24348.

32　X. Zhou, A. Q. Wang, Y. M. Pan, C. F. Yu, Y. Zou, Y. Zhou, Q. Chen and S. H. Wu, *J. Mater. Chem. A*, 2015, **3**, 13011-13015.

33　Y. Meng, K. Wang, Y. Zhang and Z. Wei, *Adv. Mater.*, 2013, **25**, 6985-6990.

34　X. M. Ma, W. Q. Zhou, D. Z. Mo, B. Y. Lu, F. X. Jiang and J. K.

RSC Advances Accepted Manuscript

Xu, *RSC Adv.*, 2015, **5**, 3215-3223.

35 R. X. Wang, Y. J. Fan, L. Wang, L. N. Wu, S. N. Sun and S. G. Sun, *J. Power Sources*, 2015, **287**, 341-348.

36 D. Billaud, B. Humbert, L. Thevenot, P. Thomas and H. Talbi, *Spectrochim. Acta Part A*, 2003, **59**, 163-168.

37 H. Takeuchi and I. Harada, *Spectrochim, Acta Part A*, 1986, **42**, 1069-1078.

38 H. Talbi, J. Ghanbaja, D. Billaud and B. Humbert, *Polymer*, 1997, **38**, 2099-2106.

39 D. Billaud, E. B. Maarouf and E. Hannecart, *Mater. Res. Bull.*, 1994, **29**, 1239-1246.

40 G. Eda and M. Chhowalla, *Adv. Mater.*, 2010, **22**, 2392-2415.

41 T. Kuila, S. Bose, A. K. Mishra, P. Khanra, N. H. Kim and J. H. Lee, *Prog. Mater. Sci.*, 2012, **57**, 1061-1105.

42 B. Gupta, D. S. Chauhan and R. Prakash, *Mater. Chem. Phys.*, 2010, **120**, 625-630.

43 C. Chen, Q. H. Yang, Y. Yang, W., Y. Lu, Wen,, P. X. Hou and H. M. Cheng, *Adv. Mater.*, 2009, **21**, 3007-3011.

44 G. Wang, J. Yang, J. Park, X. Gou, B. Wang, H. Liu and J. Yao, *J. Phys. Chem. C*, 2008, **112**, 8192-8195.

45 X. Ma, W. Zhou, D. Mo, Z. Wang and J. K. Xu, S*ynth. Met*., 2015, **203**, 98-106.

46 L. F Lai, H. P. Yang, L. Wang, B. K. Teh, J. Q. Zhong, H. Chou, L. W. Chen, W. Chen, Z. X. Shen, R. S. Ruoff and J. Y. Lin, *ACS Nano*, 2012, **6**, 5941-5951.

47 D. Sun, L. Jin, Y. Chen, J. R. Zhang and J. J. Zhu, *Chem. Plus. Chem.*, 2013, **78**, 227-234.

48 W. J. Wang, W. Lei, T. Y. Yao, X. F. Xia, W. J. Huang, Q. L. Hao and X. Wang, *Electrochim. Acta*, 2013, **108**, 118-126.

49 A. R. Liu, C. Li, H. Bai and G. Q. Shi, *J. Phys. Chem. C*, 2010, **114**, 22783-22789.

50 F. Alvi, M. K. Ram, P. Basnayaka, E. Stefanakos, Y. Goswami, A. Hoff and A. Kumar, *ECS Transactions*, 2011, **35**, 167-174.

Graphical abstract:

High-performance capacitive behavior of layered reduced graphene oxide and polyindole nanocomposite materials

Qianjie Zhou [a], Danhua Zhu [a], Xiumei Ma [a], Jingkun Xu [a, *], Weiqiang Zhou [b, *], Feng Zhao [a]

[a] Jiangxi Key Laboratory of Organic Chemistry, Jiangxi Science and Technology Normal University, Nanchang, 330013, P. R. China

[b] Chemistry and Chemical Engineering College, Jiangxi Science and Technology Normal University, Nanchang 330013, PR China

* Corresponding author: Fax: +86-791-83823320, Tel.: +86-791-88537967, E-mail: xujingkun@tsinghua.org.cn; zhouwqh@163.com
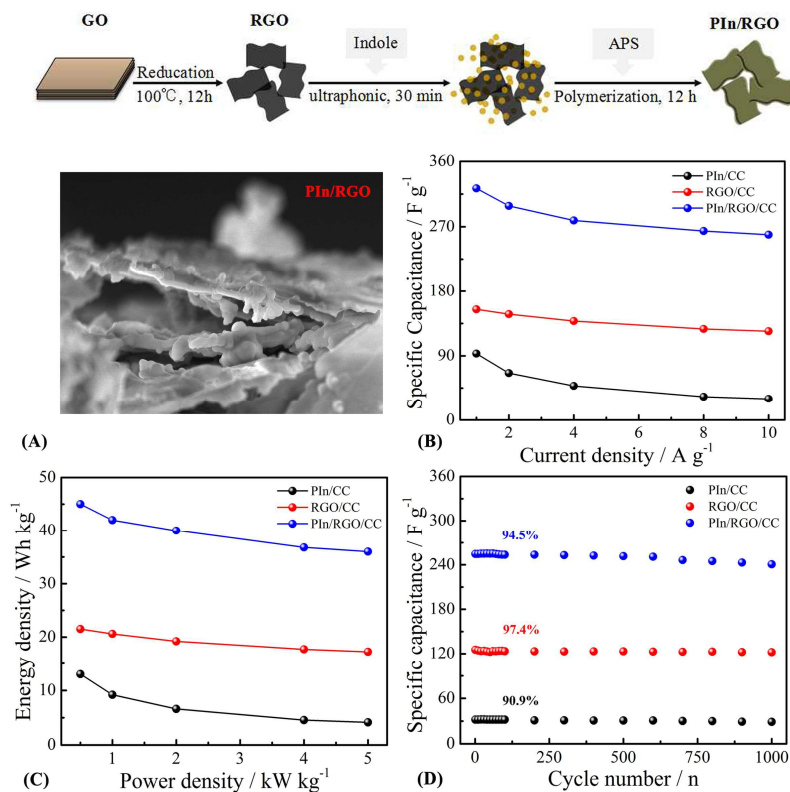
PIn/RGO hybrid nanocomposite were obtained via simple in-situ chemical oxidative polymerization based on RGO and PIn. The PIn/RGO shows a large improved specific capacitance of 322.8 F g^{-1} at a current density of 1.0 A g^{-1}, good stability with a cycling efficiency of 94.5% at a large current density of 10 A g^{-1} after 1000 cycles, and high energy density of 36 Wh kg^{-1} at high power density of 5000 W kg^{-1}. These results suggest that PIn/RGO should be a promising electrode material for supercapacitor applications.